NOLM-based wavelength conversion with FBG band-pass filter for optical packet switching

Min Zhang (张 民), Peida Ye (叶培大), Fan Zhang (张 帆), Yongpeng Zhao (赵永鹏), and Jian Wang (王 建)

BUPT-Nortel Research Center, Beijing University of Posts and Telecommunications, Beijing 100876

Received August 9, 2002

Nonlinear-optical-loop-mirror-based wavelength conversion is studied in details. A set of two-phase-shifted Bragg gratings are introduced into the coverter, serving as a narrow band-pass filter to remove new frequencies generated by walk-off and to compensate the dispersion. Numerical simulations are performed to validate our method. The results show that the converted pulses after the filter are reshaped and, sometimes, even compressed.

OCIS codes: 190.2620, 050.2770, 060.2340, 060.4370, 060.4510.

All optical wavelength conversion is a vital functionality in WDM- or TDM-based optical packet switching networks (OPS), which allows high-speed operation, transparent interoperability, contention resolution and wavelength routing[1,2].

Two kinds of wavelength converters have been identified for OPS. Wavelength converters based on semiconductor optical amplifier (SOA-WCs) are generally limited in speed and suffer bit-stream inversion, amplitude distortion, unwanted phase modulation and, consequently, SNR degradation[3,4]. In comparison, converters based on nonlinear optical loop mirror (NOLM-WCs) have proved experimentally capable of ultra-high speed and fetching performance[5,6]. However, due to walk-off and group velocity dispersion (GVD), the output pulses are broadened and distorted considerably when the difference between the original wavelength and the target wavelength increases. Therefore we made a detailed analysis of NOLM-WCs in searching for a better solution. We put a set of two-phase-shifted fiber Bragg gratings (FBGs) at the output port, which acts as a band-pass filter to remove the new frequencies generated by walk-off and to compensate GVD.

Our configuration of NOLM-WC is actually a fiber implementation of the Sagnac interferometer, shown in Fig. 1(a), where the polarization controller is omitted. At port A, a continuous-wave light at the target wavelength is divided by coupler 1 (50/50) into two counter-propagating parts, i.e. the probe and the reference. The control signal, modulated by data information, is coupled into the fiber loop via coupler 2 (10/90) and travels along the clockwise direction with the probe. Due to Kerr effect, cross phase modulation (XPM) occurs between the control signal and the probe. The latter acquires a phase shift from the reference light. When the phase shift is π, these two counter-propagating lights interfere positively at coupler 1 and can be switched out of port B completely. Thus wavelength conversion is realized. Since the optical Kerr effect in fiber is almost instantaneous, NOLM-WC can achieve very high speed.

A two-phase-shifted FBG filter[7,8], which functions as a Fabry-Perot resonator capable of wavelength selection, is integrated at port B. It consists of three uniform grating sections and two phase-shifts, shown in Fig. 1(b), where L_1 and L_2 are the lengths of the grating sections.

In order to highlight the effects of walk-off and GVD, we neglect the loss, higher-order dispersion and XPM between the reference and the control signal. Then the light propagation in the NOLM is governed by modified coupled-mode nonlinear Schrödinger equations,

$$\begin{aligned}
&\frac{\partial U_1}{\partial \xi} + \frac{L_{D1}}{L_W}\mathrm{sgn}(d)\frac{\partial U_1}{\partial \xi} + \frac{i}{2}\mathrm{sgn}(\beta_{21})\frac{\partial^2 U_1}{\partial \tau^2} \\
&\qquad = i\frac{L_{D1}}{L_{N1}}|U_1|^2 U_1, \\
&\frac{\partial U_2}{\partial \xi} + \frac{i}{2}\frac{L_{D1}}{L_{D2}}\mathrm{sgn}(\beta_{22})\frac{\partial^2 U_2}{\partial \tau^2} \\
&\qquad = i\frac{L_{D1}}{L_{N2}}(|U_2|^2 + 2|U_1|^2)U_2, \\
&\frac{\partial U_3}{\partial \xi} + \frac{i}{2}\frac{L_{D1}}{L_{D3}}\mathrm{sgn}(\beta_{23})\frac{\partial^2 U_3}{\partial \tau^2} \\
&\qquad = i\frac{L_{D1}}{L_{N3}}|U_3|^2 U_3,
\end{aligned} \tag{1}$$

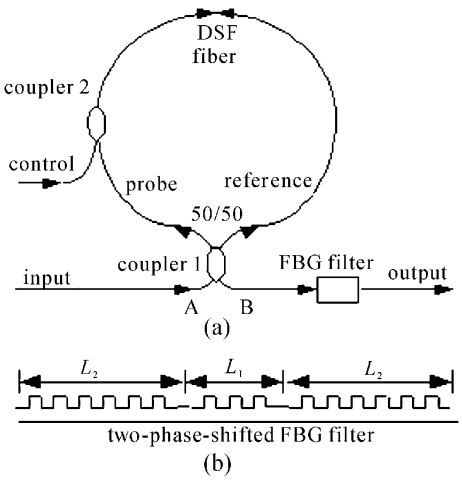

Fig. 1. Scheme of the wavelength converter based on NOLM and FBG filter.

where $\xi = z/L_{D1}, T = t - z/v_g$ and $\tau = T/T_{10}$ denote the transformation to a frame of reference moving with the control signal. T_{10} is the half-width of the control signal at $1/e$ intensity point. The subscript $k \in \{1, 2, 3\}$ indicates the control signal, the probe and the reference, respectively. β_{2k} indicates GVD. U_k is normalized amplitude. L_{Dk}, L_{Nk} and L_W are the dispersion length, the nonlinear length and the walk-off length, respectively[9].

Since the ratio of coupler 1 is 50/50, the normalized intensity of the transmitted signal (I_T) and that of the reflected signal (I_R) are given by

$$I_T = |U_2(L,T)/\sqrt{2} - iU_3(L,T)/\sqrt{2}|^2, \quad (2)$$

$$I_R = |U_2(L,T)/\sqrt{2} + iU_3(L,T)/\sqrt{2}|^2, \quad (3)$$

where the loop length should be chosen as $L = L_\pi = \pi/(2\gamma_1 P_{10})$ to provide a phase change of π between the probe and the reference.

The intensity transmission of the FBG filter is given as[7,8]

$$F(\lambda) = \frac{(1-r_1^2)^2(1-r_2^2)}{(1-r_1^2)^2(1-r_2^2) + [r_2(1+r_1^2) + 2r_1\cos(2\phi)]}, \quad (4)$$

where ϕ is the phase shift between two grating sections, $r_1 = \tanh(\kappa L_1)$ and $r_2 = \tanh(\kappa L_2)$. $\kappa = \sqrt{\gamma^2 + \delta^2}$ is the coupling coefficient of the uniform gratings. γ is the effective detuning. $\delta = 2\pi n_{\text{eff}}(1/\lambda - 1/\lambda_B)$ is the detuning from the Bragg wavelength λ_B. $\lambda_B = 2n_{\text{eff}}\Lambda$, where n_{eff} is the effective index in the gratings and Λ is the grating period.

The filter can be assumed approximately as a linear system near the center wavelength. Thus, in frequency domain, $I_{\text{out}}(w) = I_T(w) \cdot F(w)$, where I_T and $I_{\text{out}}(w)$ are the Fourier transforms of the output intensities after the NOLM and the filter, respectively. Taking the inverse transform, we can obtain the temporal output intensities.

Numerical simulations are conducted to validate our method. The algorithm of split-step fast Fourier transform is used to solve Eqs. (1). The original control signal is assumed to be unchirped hyperbolic-secant pulses, with $\lambda_1 = 1546.80$ nm, $T_{10} = 4$ ps and $P_{10} = 0.2$ W. For the purpose of better conversion effect, the average power of the probe and the reference is 4 mW, far less than P_{10}. The fiber loop consists of a dispersion shifted fiber, with $A_{\text{eff}} = 50\mu\text{m}^2$, $n_2 = 3.2 \times 10^{-20}$ m^2/W and $L_\pi \approx 3$ km.

To get a quasi-flat-top transmission spectrum, the filter is of a symmetrical structure with both phase-shifts equal to $\pi/2$. $\Lambda = 240$ nm according to $\lambda_B = 2n_{\text{eff}}\Lambda$, where $\lambda_B = 1550$ nm. Setting $F(\lambda) = 1$ and $\phi = \pi/2$, we obtain $L_2 = 2L_1$. For a given FBG filter, e.g. $\kappa = 0.02\mu\text{m}^2$, one can plot the 3-dB bandwidth against the grating strength (κL_2), where the bandwidth decreases with the increase of κL_2. Accordingly, L_2 is chosen to be 288 μm for a 3-dB bandwidth of 1.6 nm.

First, we focus upon the GVD effect on the system, taking no walk-off into account. In order to minimize the GVD mismatch, β_{21} and β_{22} are given opposite signs. As an example, GVD-induced performance degradation for $\lambda_2 = 1549.31$ nm, $\beta_{21} = -0.28$ ps^2/km and $\beta_{22} = 0.51$ ps^2/km is shown in Fig. 2(a). Without the filter, the converted pulses are broadened due to the normal dispersion. Furthermore, when GVD increases, the pulse broadening effect becomes more obviously. However, the temporal profile after the filter is compressed and can even maintain its original width, shown in Fig. 2(b). The reason is that the gratings provide anomalous dispersion to the optical pulses and compensate some of the normal dispersion. Another noteworthy finding is that, the switching contrast (I_{out}/I_R) after the filter becomes a little lower than before, since the gratings reflect some of the light. Thus, to keep a necessary extinction ratio of the output signal, the grating strength of the FBGs should not be too strong.

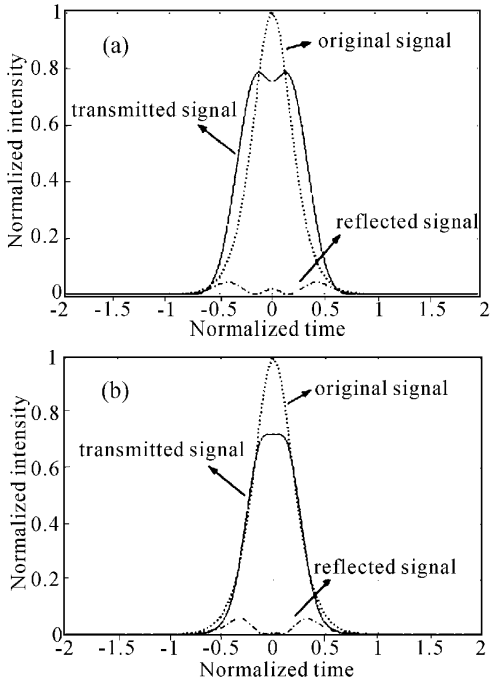

Fig. 2. Normalized intensity vs. normalized time, in case of no walk-off. $\lambda_2 = 1549.31$ nm, $\beta_{21} = -0.28$ ps^2/km and $\beta_{22} = 0.51$ ps^2/km. (a) Without FBG filter; (b) with FBG filter.

Then, we take both GVD and walk-off $d = (1/v_{g2} - 1/v_{g1})$ into consideration. λ_1 is still 1546.80 nm, while the wavelength of the probe light becomes longer gradually. Examples are shown in Fig. 3(a) for $\lambda_2 = 1555.72$ nm and $d = 2.4$ ps/km, and in Fig. 4(a) for $\lambda_2 = 1560.60$ nm and $d = 5.7$ ps/km. Obviously, the walk-off, combined with GVD, results in asymmetric spectra broadening of the output pulse and thus asymmetric temporal profile. In further study, if $d > 0$, the maximal phase-shift happens at a point where $T > 0$. Hence the switching window shifts towards $T > 0$. Conversely, If $d < 0$, the switching window shifts towards $T < 0$. Moreover, the existence of GVD prevents walk-off induced spectra broadening towards the blue side[9], so the temporal shift of the output pulse is reduced to some extent.

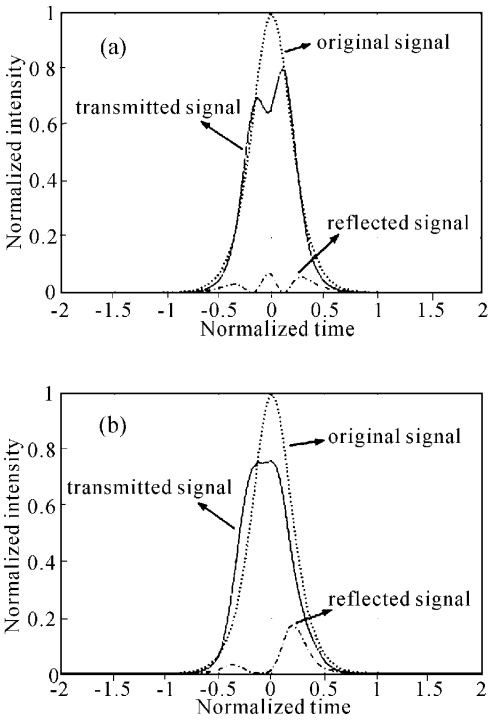

Fig. 3. Normalized intensity vs. normalized time, in case of both GVD and walk-off. $\lambda_1 = 1546.80$ nm, $\lambda_2 = 1555.72$ nm, $\beta_{21} = -0.28$ ps^2/km, $\beta_{22} = 0.51$ ps^2/km, $d = 2.4$ ps/km. (a) Without FBG filter; (b) with FBG filter.

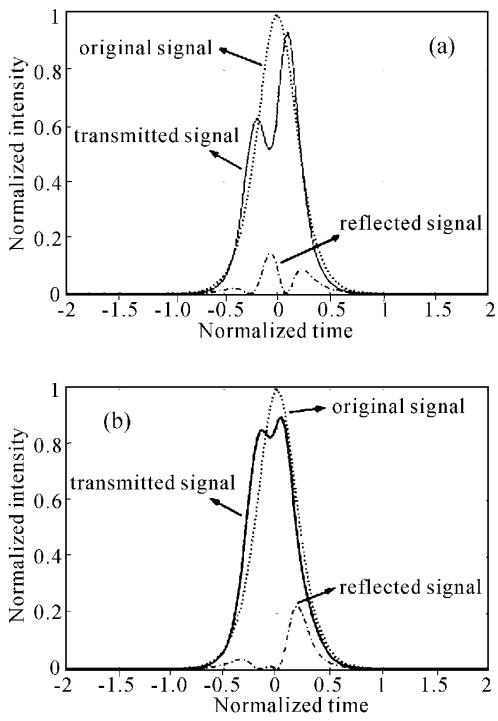

Fig. 4. Normalized intensity vs. normalized time, in case of both GVD and walk-off. $\lambda_1 = 1546.80$ nm , $\lambda_2 = 1560.60$ nm, $\beta_{21} = -1.09$ ps^2/km, $\beta_{22} = 2.45$ ps^2/km, $d = 5.7$ ps/km. (a) Without FBG filter; (b) with FBG filter.

After the FBG filter, the pulse asymmetry is smoothed and the pulse width is maintained, shown in Figs. 3(b) and 4(b). The reason is that the FBGs provide anomalous dispersion and counteracts the asymmetric spectral broadening effect in frequency domain of the probe light. However, more light component near the falling edge is reflected by the FBGs than the other part of the pulse, since the output pulse develops rapid oscillations near the falling edge while the leading edge is largely unaffected when $d > 0$. Hence, the output pulse shifts slightly towards $T < 0$. The temporal shift can be better controlled if we introduce initial time delay between the probe and the control signal[10].

In conclusion, GVD, XPM and walk-off in the NOLM-WC are analyzed in detail. By means of two-phase-shifted Bragg gratings, a narrow band-pass filter is designed to improve the performance of the NOLM-WC. The results of the numerical simulations show that the converted pulses after the FBG filter are reshaped and, sometimes, even compressed. Finally, all these results are theoretical and need to be examined by practical operation.

M. Zhang's e-mail address is zmight@hotmail.com.

References

1. J. M. H. Elmirghani and H. T. Mouftah, IEEE Comm. Mag. **38,** 86 (2000).
2. S. L. Danielsen, P. B. Hansen, and K. E. Stubkjaer, J. Lightwave Technol. **16,** 2095 (1998).
3. M. Saitoh, B. Ma, and Y. Nakano, IEEE J. Quantum Electron. **36,** 984 (2000).
4. M. W. K. Mak, H. K. Tsang, and K. Chan, IEEE Photon. Technol. Lett. **12,** 525 (2000).
5. J. P. Hemingway and A. L. Steele, IEEE J. Selected Topics in Quantum Electron. **3,** 1246 (1997).
6. J. Yu, P. Jeppesen, and S. N. Knudsen, Electron. Lett. **37,** 577 (2001).
7. L. Wei and J. W. Y. Lit, J. Lightwave Technol. **15,** 1405 (1997).
8. R. Kashyap, *Fiber Bragg Gratings* (Academic Press, San Diego, 1999), p.229.
9. G. P. Agrawal, *Nonlinear Fiber Optics,* 2nd Edition (Academic Press, San Diego, 1995), p.60, p.277.
10. X. Liu and P. Ye, J. Opt. Commun. **21,** 178 (2000).